# Supporting Information

## Room temperature ammonia gas sensing using mixed-valent $CuCo_2O_4$ nano-platelets: Performance enhancement through stoichiometry control

*Srashti Jain[1#], Apurva Patrike[1#], Satish S. Badadhe[1], Monika Bhardwaj[1*] and Satishchandra Ogale[1*].*

[1]Department of Physics and Centre for Energy Science, Indian Institute of Science Education and Research, Pune 411008-India

#Equal contribution

***Corresponding authors**

Satishchandra Ogale Email: satishogale@iiserpune.ac.in, satishogale@gmail.com

Monika Bhardwaj, Email: bharadwajmonika03@gmail.com

**Keywords:** Ternary oxide, off-Stoichiometry, nanowalls, room temperature, sensing, $NH_3$.

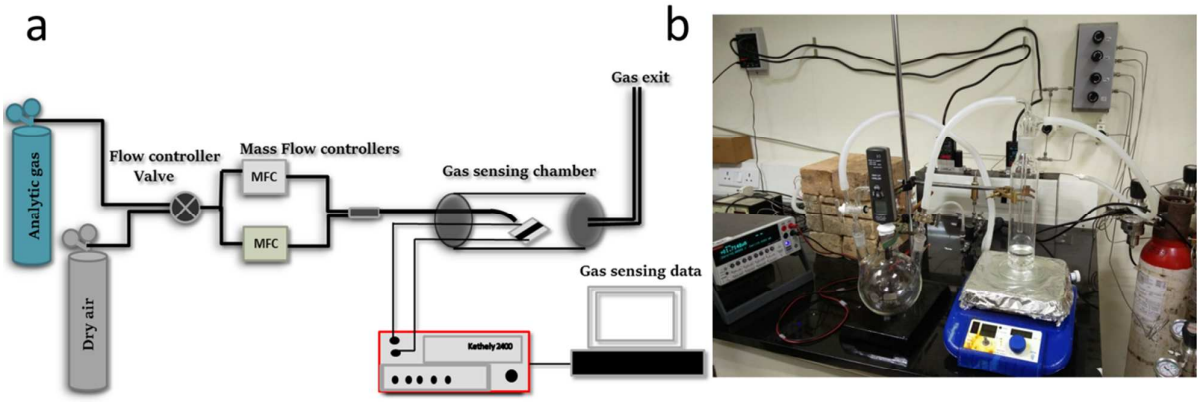


**Figure S1** (a)Schematic diagram (b) Laboratory gas sensing set up

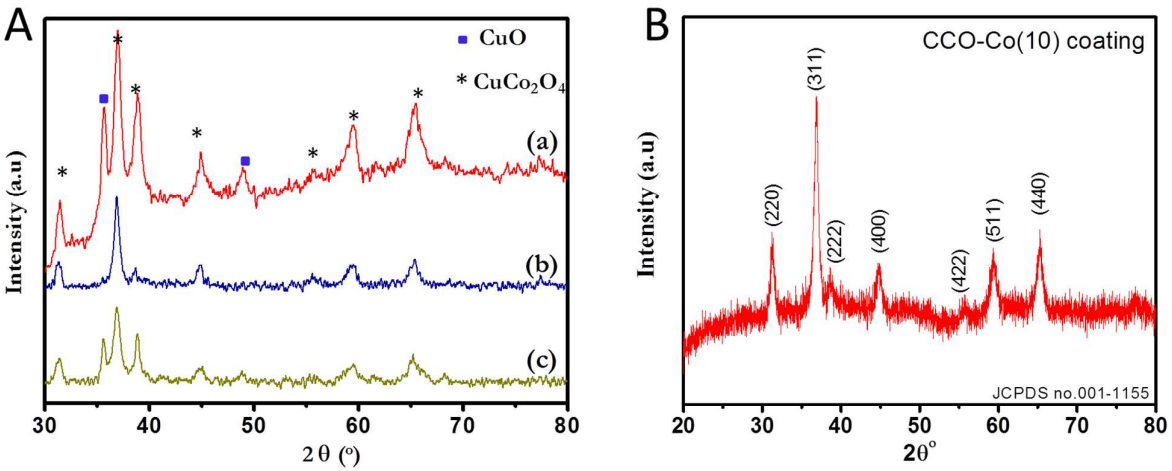


**Figure S2: (A)** X-ray diffraction data for the samples (a) CCO-S (stoichiometric concentration of precursors in reaction vessel), (b) CCO-Co (10 at%. excess cobalt precursor), and (c) CCO-Cu (10 at.% excess copper precursor) (B) X-ray diffraction pattern of CCO-Co(10) coating used for sensing in present work.

[Figure S2(A) is reprinted from Materials Research Bulletin, 90 / n/a, Monika Bhardwaj, Anil Suryawanshi, Rohan Fernandes, Surendar Tonda, Abhik Banerjee, Dushyant Kothari, Satishchandra Ogale, $CuCo_2O_4$ nanowall morphology as Li-ion battery anode: Enhancing electrochemical performance through stoichiometry control, 303-310., Copyright (2017), with permission from Elsevier]

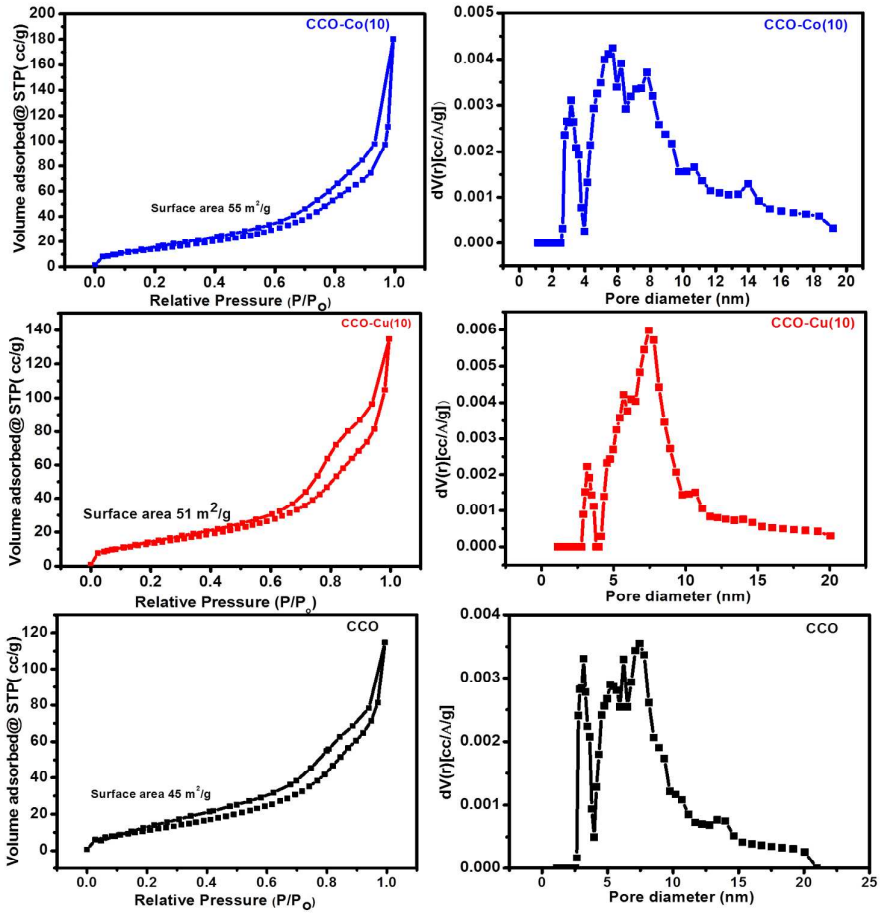


**Figure S3.** BET graphs and pore size distribution of respective sensing materials

**Table S1**. A comparative analysis of gas sensing response of different materials.

| Metal oxides | $NH_3$(ppm) | Temp. | Response time | Response/formula used | Ref. |
|---|---|---|---|---|---|
| $In_2O_3$ | 20 | RT | <20s | $2500/(\Delta R/R_o*100)$ | (1) |
| NiO | 30 | RT | 27 s/ (recovery in IR lamp) | $0.3/(\Delta R/R_o)$ | (2) |
| NiO/ZnO | 50 | RT | 30 s | $0.5/(\Delta R/R_o)$ | (3) |
| Beta-$Ga_2O_3$ | 0.5 | RT | 40 s | $19/(\Delta R/R_o*100)$ | (4) |
| CNT | 100 | RT | 60 s (not complete recovery) | $0.25/(\Delta R/R_o)$ | (5) |
| **CCO-Co(10)** | **400** | **RT** | **120 s** | **$7.9/(\Delta R/R_o*100$** | **This work** |
| $SnO_2$/MWCNT | 1000 | RT | <300 s | 27.5/(Rg/Ra) | (6) |
| Au-CNT | 500 | RT | 300 s | $4.18(\Delta R/R_a* 100)$ | (7) |
| CuO | 100 | 200°C | 360 s | $3 (R_g/R_a)$ | (8) |
| $Fe_2O_3$-ZnO | 0.4 | RT | 500s/70 s | 80/(Ig/Ia) | (9) |
| SWCNT | 40 | RT | 10 min | $5 (\Delta R/R_a* 100)$ | (10) |
| CuO | 60 | 250°C | 13 min | $19.85 (\Delta R/R_a* 100)$ | (11) |
| PANI | 92 | RT | 13.9 min | $7.10(\Delta R/R_a* 100)$ | (12) |
| PPy-$TiO_2$/ZnO | 450 | RT | 15 min | $35(\Delta R/R_a* 100)$ | (13) |
| $Co_3O_4$ | 50 | 240°C | 21 min | $31 (\Delta R/R_a)$ | (14) |

**Gas sensing mechanism**

The gas sensing mechanism in the present case can be described by using adsorption of oxygen molecules on the surface of oxides and subsequent reaction of adsorbed oxygen molecules with analyte gas molecules. At low temperature <150°C, the adsorbed oxygen has $O_2^-$ character[15] while it possesses $O^-$ character in the temperature range between 150°C and 400°C. Above 400°C oxygen has the $O^{2-}$ character. Therefore The gas sensing mechanism at room temperature (23°C in this case) is predominantly due to the reaction between $O_{2(ads)}^-$ and analyte gas molecules.

The gas sensing performance is governed by two processes namely the receptor function and the transducer function which involves interaction of the analyte with a sensor which results in variation in charge carriers and subsequent transport of these charge carries in the sensor.[16] In the present case, nanoporous nanoplatelets are constituted by nanograin particles. The electronic transport between nanograins is governed by grain boundary barrier. Apart from that different factors such as trap states at the grain boundaries and defect states in the semiconductor can also affect the electron transport between the nanograins. The gas sensing mechanism for nanograins based p-type sensor can also be explained using variation in the charge accumulation layer around the nanograins and potential barrier between nanograins (Figure 4) S4 p-type materials, adsorption of oxygen species on the nanograin surface leads to abstraction of electrons from the surface resulting in the formation holes. These holes present beneath the surface of nanograins lead to the formation of a hole-accumulation layer around the nanograins [Figure 4(a)]. Therefore, transport takes place through a hole-accumulated layer around the grains (shown by the red arrow in Figure 4). Thus, increase in the width of a hole-accumulation layer leads to a decrease in the potential barrier for holes, facilitating the charge transport. When reducing gas (here, $NH_3$) is passed over the sensor, the reducing gas interacts with the adsorbed oxygen anions which lead to the removal of oxygen from the sensor surface, releasing the electrons back into the nanograins. Thus the electrons and holes recombine which leads to a reduction in the width of the hole accumulation layer and increases the potential barrier height between the grains for hole transport due to which the resistance of the sensor increases [Figure 4(b)].

When an oxidizing gas (like $NO_2$) is passed over the sensor, the width of a hole accumulation layer further increases by the extraction of the electrons from the nanograins; as a result, the sensor resistance decreases due to the increase in the electronic transport channel around the grain. The simplified surface reactions for $NH_3$ and $NO_2$ are given as follows[2],

$$4\,NH_3 + 3O_{2(ads)}{}^- \Rightarrow 2N_2 + 6H_2O + 3e^- \quad (1)$$

$$2NH_3 + 3O_{(ads)}{}^- \Rightarrow N_2 + 3H_2O + 3e^- \quad (2)$$

$$NO_2 + e^- \Rightarrow NO_{(g)} + O_{(ads)}{}^- \quad (3)$$

$$NO_2 + O_{2(ads)}{}^- + 2e^- \Rightarrow NO_{2(ads)}{}^- + 2O_{(ads)}{}^- \quad (4)$$

Similar kinds of gas sensing reactions take place in the case of CCO and CCO-Cu(10).

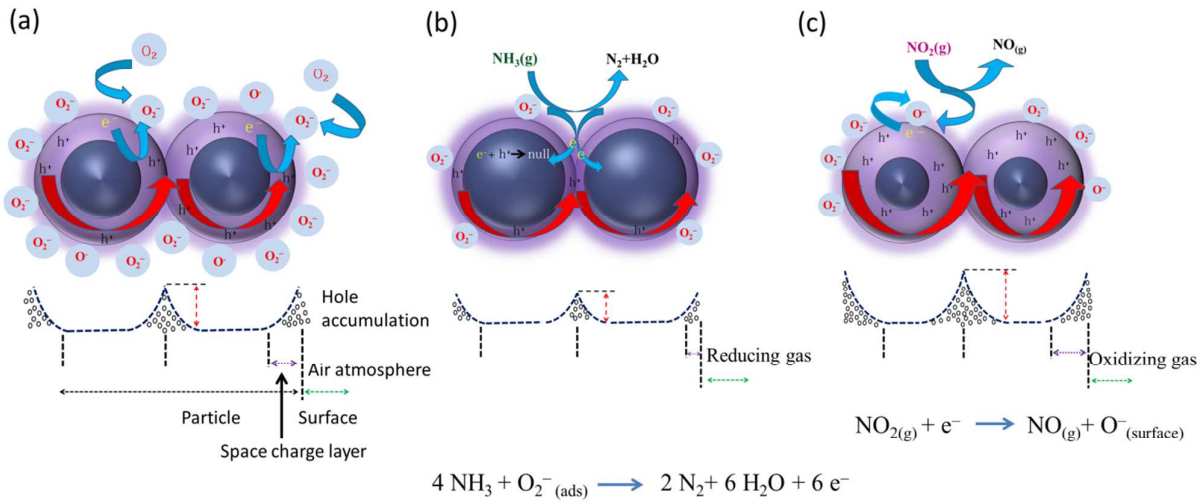


**Figure S 4**.(a, b, c) Schematics illustrating gas sensing mechanism in the presence of reducing and oxidizing gases.

**References:**


(1) Du, N.; Zhang, H.; Chen, B.; Xiangyang, M.; Liu, Z.; Wu, J.; Yang, D. Porous indium oxide nanotubes: Layer-by-layer assembly on carbon-nanotube templates and application for room-temperature NH3 gas sensors. *Adv. Mater.* **2007**, *19* (12), 1641–1645

(2) Wang, J.; Yang, P.; Wei, X.; Zhou, Z. Preparation of NiO two-dimensional grainy films and their high-performance gas sensors for ammonia detection. *Nanoscale Res. Lett.* **2015**, *10* (1), 1–6

(3) Wang, J.; Yang, P.; Wei, X. High-performance, room-temperature, and no-humidity-impact ammonia sensor based on heterogeneous nickel oxide and zinc oxide nanocrystals. *ACS Appl. Mater. Interfaces* **2015**, *7* (6), 3816–3824

(4) Pandeeswari, R.; Jeyaprakash, B. G. High sensing response of β-Ga2O3 thin film towards ammonia vapours: Influencing factors at room temperature. *Sensors Actuators, B Chem.* **2014**, *195*, 206–214

(5) Bekyarova, E.; Davis, M.; Burch, T.; Itkis, M. E.; Zhao, B.; Sunshine, S.; Haddon, R. C. Chemically functionalized single-walled carbon nanotubes as ammonia sensors. *J. Phys. Chem. B* **2004**, *108* (51), 19717–19720

(6) Van Hieu, N.; Thuy, L. T. B.; Chien, N. D. Highly sensitive thin film NH3 gas sensor operating at room temperature based on SnO2/MWCNTs composite. *Sensors Actuators, B Chem.* **2008**, *129* (2), 888–895

(7) Randeniya, L. K.; Martin, P. J.; Bendavid, A.; McDonnell, J. Ammonia Sensing Characteristics of Carbon-Nanotube Yarns Decorated with Nanocrystalline Gold. *Carbon* **2011**, *49* (15),

5265–5270.
(8) Shao, F.; Hernández-ramírez, F.; Prades, J. D.; Fàbrega, C.; Andreu, T.; Morante, J. R. Applied Surface Science Copper ( II ) Oxide Nanowires for P-Type Conductometric NH 3 Sensing. **2014**, *311* (Ii), 177–181.
(9) Tang, H.; Yan, M.; Zhang, H.; Li, S.; Ma, X.; Wang, M.; Yang, D. A selective NH3 gas sensor based on Fe2O3–ZnO nanocomposites at room temperature. *Sensors Actuators B Chem.* **2006**, *114* (2), 910–915
(10) Quang, N. H.; Van Trinh, M.; Lee, B.; Huh, J. Effect of NH3 Gas on the Electrical Properties of Single-Walled Carbon Nanotube Bundles. *Sensors and Actuators B: Chemical* **2006**, *113* (1), 341–346.
(11) Duc Hoa, N.; Van Quy, N.; Anh Tuan, M.; Van Hieu, N. Facile Synthesis of P-Type Semiconducting Cupric Oxide Nanowires and Their Gas-Sensing Properties. *Physica E: Low-Dimensional Systems and Nanostructures* **2009**, *42* (2), 146–149.
(12) Kebiche, H.; Debarnot, D.; Merzouki, A.; Poncin-Epaillard, F.; Haddaoui, N. Relationship between Ammonia Sensing Properties of Polyaniline Nanostructures and Their Deposition and Synthesis Methods. *Analytica Chimica Acta* **2012**, *737*, 64–71.
(13) Wang, Y.; Jia, W.; Strout, T.; Schempf, A.; Zhang, H.; Li, B.; Cui, J.; Lei, Y. Ammonia Gas Sensor Using Polypyrrole-Coated TiO2/ZnO Nanofibers. *Electroanalysis* **2009**, *21* (12), 1432–1438.
(14) Wöllenstein, J.; Burgmair, M.; Plescher, G.; Sulima, T.; Hildenbrand, J.; Böttner, H.; Eisele, I. Cobalt Oxide Based Gas Sensors on Silicon Substrate for Operation at Low Temperatures. *Sensors and Actuators, B: Chemical* **2003**, *93* (1–3), 442–448.
(15) Barsan, N.; Weimar, U. Conduction Model of Metal Oxide Gas Sensors. *Journal of Electroceramics* **2001**, *7* (3), 143–167.
(16) Dong, G.; Fan, H.; Tian, H.; Fang, J.; Li, Q. Gas-Sensing and Electrical Properties of Perovskite Structure P-Type Barium-Substituted Bismuth Ferrite. *RSC Adv.* **2015**, *5* (38), 29618–29623.